RESEARCH ARTICLE

annalen der physik
www.ann-phys.org

Spectral Structure and Doublon Dissociation in the Two-Particle Non-Hermitian Hubbard Model

Stefano Longhi

Strongly-correlated systems in non-Hermitian models are an emergent area of research. Herein, a non-Hermitian Hubbard model is considered, where the single-particle hopping amplitudes on the lattice are not reciprocal, and provide exact analytical results of the spectral structure in the two-particle sector of Hilbert space under different boundary conditions. The analysis unveils some interesting spectral and dynamical effects of purely non-Hermitian nature and that deviate from the usual scenario found in the single-particle regime. Specifically, a spectral phase transition of the Mott-Hubbard band on the infinite lattice is predicted as the interaction energy is increased above a critical value, from an open to a closed loop in complex energy plane, and the dynamical dissociation of doublons, i.e., instability of two-particle bound states, in the bulk of the lattice, with a sudden revival of the doublon state when the two particles reach the lattice edge. Particle dissociation observed in the bulk of the lattice is a clear manifestation of non-Hermitian dynamics arising from the different lifetimes of single-particle and two-particle states, whereas the sudden revival of the doublon state at the boundaries is a striking burst edge dynamical effect peculiar to non-Hermitian systems with boundary-dependent energy spectra, here predicted for the first time for correlated particles.

1. Introduction

The Hubbard model[1] provides a powerful theoretical model in condensed matter physics and related fields, such as ultracold atomic physics, that describes interacting electrons in a lattice. Since its introduction more than half a century ago, it has become a cornerstone of many studies, particularly in the field of strongly correlated systems (see e.g., [2–4] and references therein). The Hubbard model considers a lattice of sites and assumes that electrons can hop between neighboring lattice sites, with a Coulomb interaction occurring only when two electrons with opposite spins occupy the same site. The interplay between electron hopping and electron–electron interactions gives rise to a complex and rich phase diagram with various phases, such as unconventional superconductivity, Mott insulators, and density-wave ordering, depending on the values of the hopping amplitude, the interaction strength, and the electron filling.[4] Even in the simplest case of two interacting electrons with opposite spins, the Hubbard model displays an interesting physics, such as the formation of the Mott-Hubbard band describing doublons, i.e., pairs of bound repulsive electrons occupying the same lattice site.[5–12] For sufficiently strong repulsion, doublons represent stable quasiparticles that undergo correlated tunneling on the lattice and cannot dissociate owing to energy conservation.[13,14]

Recently, an enormous and increasing interest has been devoted to the study of non-Hermitian models, where the Hamiltonian of the system is described by a non self-adjoint operator.[15–21] Effective non-Hermiticity originates from exchanges of particles or energy with the external environment and gives rise to unusual and counterintuitive phenomena that are not present in Hermitian systems,[15–55] such as novel topological phases and phase transitions,[16–18,21,22,24,25,30,32,39] exceptional points and lines,[20,54,55] the non-Hermitian skin effect,[18,22,26,27,29,34,39,54] a generalized bulk-boundary correspondence principle,[18,23,26,31,35,38,43] and a wide variety of dynamical signatures and phenomena.[34,37,50–53] Non-Hermitian extensions of the Hubbard and related models have been considered in some recent works.[56–67] Different forms of the non-Hermitian Hubbard model have been introduced, which depend on the specific non-Hermitian terms included in the Hamiltonian. Generally, they can involve non-reciprocal hopping terms between lattice sites, complex on-site energies, or complex electron–electron interaction terms. Most previous studies on non-Hermitian Hubbard models focused on the issues of non-Hermitian many-body localization in the presence of disorder, the interplay between correlation and the non-Hermitian skin effect, and many-body non-Hermitian topology. Studying the non-Hermitian Hubbard model involves analyzing the eigenvalues and eigenvectors of the Hamiltonian to understand the system energy levels and wavefunctions, their topological properties and novel phase transitions. The complexity of the analysis prevents rather generally

S. Longhi
Dipartimento di Fisica
Politecnico di Milano
Piazza L. da Vinci 32, I-20133 Milano, Italy
E-mail: stefano.longhi@polimi.it
S. Longhi
IFISC (UIB-CSIC)
Instituto de Fisica Interdisciplinar y Sistemas Complejos, E-07122
Palma de Mallorca, Spain

The ORCID identification number(s) for the author(s) of this article can be found under https://doi.org/10.1002/andp.202300291

DOI: 10.1002/andp.202300291

to obtain exact analytical results, and large-scale numerical simulations are required even when dealing with few particles. The study of simple models allowing for exact analytical results is thus of main relevance and interest. On the experimental side, doublon dynamics has been demonstrated in different physical platforms, including ultracold atoms in optical lattices[5,13,14,68,69] and classical simulators of two- or three-particle dynamics in Fock space based on photonic[70] or topolectrical[71,72] lattices with engineered defects. The current advances in experimental fabrication and control of synthetic matter, including the ability to realize non-reciprocal hopping, make it possible to realize few- body non-Hermitian Hubbard models in a laboratory,[72] thus motivating the study of correlated particle states and doublon dynamics in non-Hermitian models.

The simplest non-Hermitian version of the Hubbard model was introduced in Ref. [56] (see also [60, 61, 63]) and considers non-reciprocal single-particle hopping amplitudes arising from an imaginary gauge field. It can be regarded as a many-body generalization of the Hatano-Nelson model[73–75] for interacting particles, and can be thus referred to as the interacting Hatano-Nelson model. The Hatano-Nelson model provides a paradigmatic non-Hermitian model displaying a nontrivial point-gap topology and the non-Hermitian skin effect in the single-particle case.[18] One of the major results of single-particle band theory in models displaying the non-Hermitian skin effect is the strong dependence of the energy spectrum on the boundary conditions. Rather generally, under periodic boundary conditions (PBC) or in the infinite lattice limit (ILL) the energy spectrum is described by a set of closed loops in complex energy plane; under open boundary conditions (OBC) the energy spectrum shrinks into a set of open arcs embedded in the ILL energy loops; finally, under semi-infinite boundary conditions (SIBC) the energy spectrum is described by an area in complex energy plane whose contours are the ILL energy loops (see e.g. [39, 50]). As the spectral and topological properties of the interacting Hatano-Nelson model under PBC have been numerically investigated in previous works,[60,61] an open question is the dependence of the energy spectrum on the boundary conditions, either PBC, OBC, or SIBC, and specifically how the general scenario found in the single-particle case[39] changes in the many-particle regime. Also, the impact of non-reciprocal coupling on the dynamical behavior of correlated particles, such as correlated hopping and the stability of doublons, has been so far overlooked.

In this work we consider the interacting Hatano-Nelson model in the two-particle sector and unveil emergent spectral and dynamical regimes arising from the interplay between particle correlations and the non-Hermitian gauge potential, which have been so far overlooked. By a suitable extension of the Bethe Ansatz for the non-Hermitian Hubbard model, we provide an exact analytical form of the energy spectrum for different types of boundary conditions and unveil a new spectral phase transition of theMott-Hubbard band of purely non-Hermitian nature when the interaction strength is increased above a critical value. Finally, we predict a novel dynamical regime of correlated particles without anyHermitian counterpart, namely doublon dissociation in the bulk of the lattice and sudden doublon resurgence at the lattice edges. Particle dissociation observed in the bulk of the lattice arises from the longer lifetime of single-particle states over two-particle states, and it is thus a very distinct phenomenon that particle delocalization observed in the single-particle Hatano-Nelson model with disorder.[73–75] On the other hand, the sudden resurgence of the doublon state at the lattice boundaries are a striking boundary-induced dynamical phenomenon peculiar to non-Hermitian systems displaying the non-Hermitian skin effect,[51,52] here demonstrated for the first time for correlated particle states.

2. The Non-Hermitian Hubbard Model for Two Interacting Particles

The starting point of our analysis is provided by a non-Hermitian extension of the Hubbard model,[56,61] also referred to as the interacting Hatano-Nelson model, which describes the hopping dynamics of interacting fermionic particles in a 1D tight-binding lattice subjected to an imaginary gauge field. We indicate by $J > 0$ the single-particle hopping amplitude between adjacent sites in the lattice, by $h \geq 0$ the imaginary gauge field, and by U the on-site interaction energy of fermions with opposite spins ($U > 0$ for a repulsive interaction). The effective non-Hermitian Hubbard Hamiltonian of the system reads[56,61]

$$\hat{H} = -\sum_{l,\sigma}\left(J\exp(h)\hat{a}^{\dagger}_{l,\sigma}\hat{a}_{l+1,\sigma} + J\exp(-h)\hat{a}^{\dagger}_{l+1,\sigma}\hat{a}_{l,\sigma}\right) + U\sum_{l}\hat{n}_{l,\uparrow}\hat{n}_{l,\downarrow} \tag{1}$$

where $\hat{a}_{l,\sigma}$, $\hat{a}^{\dagger}_{l,\sigma}$ are the annihilation and creation operators of fermions with spin $\sigma = \uparrow, \downarrow$ at lattice site l, $\hat{n}_{l,\sigma} = \hat{a}^{\dagger}_{l,\sigma}\hat{a}_{l,\sigma}$ is the particle-number operator, and h is the imaginary gauge field (magnetic flux). In the limit $U = 0$, the model reduces to the many-particle non-interacting Hatano-Nelson model, whereas for $h = 0$ it reduces to the standard (Hermitian) Hubbard model. For pure states and considering open-system dynamics conditioned on measurement outcomes such that the quantum evolution corresponds to the null-jump process, the state vector $|\psi(t)\rangle$ of the system at time t reads (see e.g., [57, 76–79])

$$|\psi(t)\rangle = \frac{\exp(-i\hat{H}t)|\psi(0)\rangle}{\|\exp(-i\hat{H}t)|\psi(0)\rangle\|} \equiv \frac{|\Phi(t)\rangle}{\||\Phi(t)\rangle\|} \tag{2}$$

where we have set $|\Phi(t)\rangle \equiv \exp(-iHt)|\psi(0)\rangle$. Basically, at each time interval dt the state vector evolves according to the Schrôdinger equation with an effective non-Hermitian Hamiltonian $\hat{H}$, followed by a normalization of the wave function, without undergoing any quantum jump.[57,76–79]

In the single-particle sector of Hilbert space, the Hamiltonian (1) describes the well-known disorder-free Hatano-Nelson model,[73–75] which provides a paradigmatic model displaying the non-Hermitian skin effect, a nontrivial point-gap topology and a strong dependence of its energy spectrum on the boundary conditions (see e.g., [16, 18, 39]). In this work, we will focus our analysis by considering two fermions with opposite spins. In this case, we can expand $|\Phi(t)\rangle$ in Fock space according to

$$|\Phi(t)\rangle = \sum_{n,m}\phi_{n,m}(t)\hat{a}^{\dagger}_{n,\uparrow}\hat{a}^{\dagger}_{m,\downarrow}|0\rangle \tag{3}$$

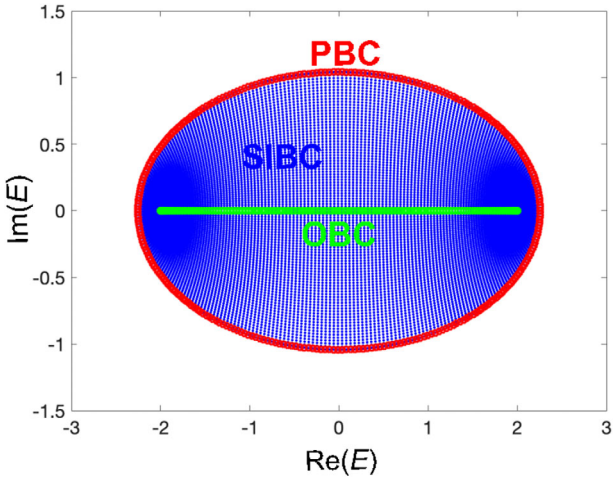

Figure 1. Energy spectrum $\sigma(H)$ in complex energy plane of the single-particle non-Hermitian Hubbard model (Hatano-Nelson model) under different boundary conditions. The outer red loop (ellipse) is the energy spectrum $\sigma(H_{PBC})$ (or $\sigma(H_{ILL})$) under PBC, the straight segment on the real energy axis is the OBC energy spectrum $\sigma(H_{OBC})$, whereas the shaded blue area is the SIBC energy spectrum $\sigma(H_{SIBC})$. Parameter values are $J = 1$ and $h = 0.5$.

where $|\phi_{n,m}(t)|^2$ is the (non-normalized) probability that the two electrons with spin ↑ and ↓ occupy the two sites n and m of the lattice, respectively. The evolution equations of the amplitudes $\phi_{n,m}(t)$ read

$$i\frac{d\phi_{n,m}}{dt} = -J\exp(h)\left(\phi_{n+1,m} + \phi_{n,m+1}\right) - J\exp(-h)\left(\phi_{n-1,m} + \phi_{n,m-1}\right) + U\phi_{n,m}\delta_{n,m} \quad (4)$$

3. Energy Spectrum

Let us first briefly remind the spectral properties in the single-particle sector of Hilbert space, where the non-Hermitian Hubbard model reduces to the clean (disorder-free) Hatano-Nelson model. The results are summarized in **Figure 1** (see e.g., [16, 18, 39] for details). The energy spectrum $\sigma(H_{ILL})$ on the infinite lattice (or equivalently under PBC) is given by

$$E = -2J\cos(k - ih) \quad (5)$$

where k is the Bloch wave number, that can take real values and varies in the range $-\pi \le k \le \pi$. Clearly, the energy spectrum under PBC describes a closed loop (an ellipse) in complex energy plane (solid red curve in Figure 1). The corresponding eigenfunctions are plane waves with a real wave number k. Under OBC, the energy spectrum $\sigma(H_{OBC})$ is entirely real, independent of the imaginary gauge field h, and reads (green solid curve in Figure 1)

$$E = -2J\cos(k) \quad (6)$$

$(-\pi \le k \le \pi)$; the corresponding eigenfunctions are squeezed toward one edge of the lattice (non-Hermitian skin effect). Finally, under SIBC the energy spectrum $\sigma(H_{SIBC})$ reads (shaded blue area in Figure 1)

$$E = -2J\cos(k - ih) \quad (7)$$

where now the wave number k is complex satisfying the constraint $0 \le \mathrm{Im}(k) \le 2h$. In complex energy plane, the SIBC energy spectrum describes the entire area (ellipse) enclosed by the PBC energy loop, and the corresponding wave functions are extended when k is real and squeezed toward the edge of the semi-infinite lattice when k is complex. We mention that each SIBC edge eigenstate, with eigenenergy E internal to the PBC energy loop, is predicted from a bulk-boundary correspondence principle[16,39] and should not be regarded as a mere mathematical object, because it can be selectively excited and it is thus of physical relevance.[50,80]

In the two-particle sector of Hilbert space, the energy spectrum E and corresponding eigenstates $u_{n,m}$ of the non-Hermitian Hubbard Hamiltonian are obtained by solving the spectral problem

$$Eu_{n,m} = -J\exp(h)\left(u_{n+1,m} + u_{n,m+1}\right) - J\exp(-h)\left(u_{n-1,m} + u_{n,m-1}\right) + Uu_{n,m}\delta_{n,m} \quad (8)$$

with suitable boundary conditions. The eigenstates can be classified as symmetric or antisymmetric for particle exchange, i.e., $u_{n,m} = u_{m,n}$ or $u_{n,m} = -u_{m,n}$. Clearly, since for an antisymmetric eigenfunction one has $u_{n,n} = 0$, the interaction term U does not influence the energy spectrum. Hence, for antisymmetric states the spectrum can be simply retrieved from the spectrum of the single particle problem. Conversely, the interaction term is important for symmetric states. Therefore, in the following, we will limit to consider the energy spectrum arising from the wave functions which are symmetric under particle exchange, i.e., we impose the further condition $u_{n,m} = u_{m,n}$ to Equation (8).

The energy spectrum in the Hermitian limit $h = 0$ is exactly solvable using the Bethe-Ansatz method.[3] Usually, the solution is searched by assuming a lattice of finite size L with either PBC or OBC, which provide suitable quantization conditions of wave numbers via the Lieb-Wu equations.[3] However, a much simpler situation occurs when considering an infinite lattice and the solutions on the infinite interval,[3,6,81,82] which do not require quantization of the wave numbers. In this case, the energy spectrum is absolutely continuous and composed by two branches, corresponding to (i) the scattering states of asymptotically free particles (E_1-branch), and (ii) interaction-bound dimer states (doublons; E_2-branch).[3,6] The energy spectrum of scattering states (E_1-branch) is simply given by

$$E_1(k_1, k_2) = -2J\cos k_1 - 2J\cos k_2 \quad (9)$$

where k_1, k_2 are arbitrary real wave numbers (quasi momenta) of the two asympotically-free fermions. This spectrum is precisely the one found for two non-interacting particles; when considering both symmetric and antisymmetric states, this implies that the above energies are doubly degenerate (the degeneracy is lifted for a finite size L of the lattice[3]). For the symmetric states,

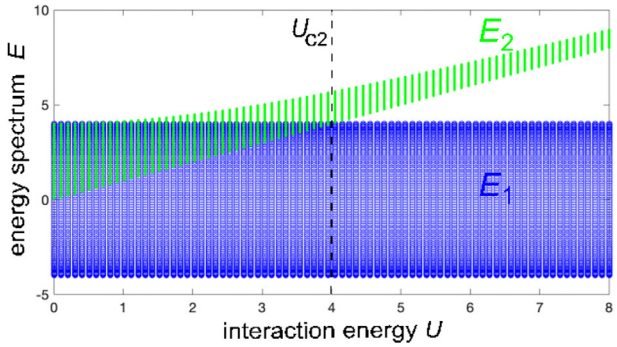

Figure 2. Energy spectrum $\sigma(H)$ of the two-particle Hubbard model in the Hermitian limit $h = 0$ versus the interaction energy U for $J = 1$. The spectrum comprises two branches, E_1 and E_2 branches, corresponding to asymptotically two-particle free scattering states and bound two-particle states (doublons), respectively. An energy gap appears as U is increased above the critical value $U_{c2} = 4J$. In the non-Hermitian regime $h > 0$, the same spectrum is obtained under OBC.

we have the additional energy spectrum describing the bound-particle state (doublon) branch (E_2-branch), given by

$$E_2(q) = \sqrt{U^2 + 16J^2\cos^2(q)} \tag{10}$$

where $q = (k_1 + k_2)/2$ is the real wave number of the particle center of mass. The latter branch corresponds to the well-known Mott-Hubbard band, with the formation of a gap when the interaction energy U is larger than the critical value $U_{c2} = 4J$; see **Figure 2**. Clearly, in the Hermitian limit the above results can be obtained from the finite lattice model, with either PBC or OBC, in the thermodynamic limit $L \to \infty$.

The situation drastically changes when we consider the non-Hermitian Hubbard model with a non-vanishing imaginary gauge field $h > 0$, which makes the energy spectrum $\sigma(H)$ strongly dependent on the boundary conditions even in the absence of particle interaction (see e.g., [16, 18, 28, 29, 39]). In the following analysis, we will provide exact results of the energy spectrum $\sigma(H)$ for $U > 0$ in the two-particle sector of Hilbert space by considering three different boundary conditions:

(i) OBC: a finite lattice comprising L sites with OBC in the large L limit. In this case the spectral problem (8) is defined on the domain $n, m = 1, 2, \ldots, L$ with the boundary conditions

$$u_{0,m} = u_{n,0} = u_{L+1,m} = u_{n,L+1} = 0 \tag{11}$$

(ii) ILL: the infinitely-extended lattice, where the lattice indices n and m vary over the entire infinite interval $(-\infty, \infty)$. In this case the spectral problem (8) is supplemented by the condition that $|u_{n,m}|$ remains bounded as $n, m \to \pm\infty$, i.e.,

$$\text{Suplim}_{n,m\to\pm\infty}|u_{n,m}| < \infty \tag{12}$$

We mention that the ILL boundary conditions greatly simplify the analysis than considering more common PBC on a finite lattice of size L, in the large L limit. We will check by numerical simulations that, as one would expect by considering the $U = 0$ limit, the PBC energy spectrum in the large L limit is reproduced by the ILL energy spectrum, which can be calculated in an exact form.

(iii) SIBC: a semi-infinite lattice. In this case the spectral problem (8) is defined over the semi-plane $n, m = 1, 2, 3, \ldots$ with the boundary conditions

$$u_{0,m} = u_{n,0} = 0 \tag{13}$$

and

$$\text{Suplim}_{n,m\to+\infty}|u_{n,m}| < \infty \tag{14}$$

3.1. Energy Spectrum Under Open Boundary Conditions

Assuming OBC, the spectral problem defined by Equations (8) and (11) can be readily solved by introduction of a non-unitary transformation of the wave function, which reduces the analysis to the ordinary (Hermitian) Hubbard model. After letting

$$u_{n,m} = w_{n,m}\exp(-hn - hm) \tag{15}$$

from Equation (8) one obtains

$$Ew_{n,m} = -J\big(w_{n+1,m} + w_{n,m+1} - w_{n-1,m} + w_{n,m-1}\big) + Uw_{n,m}\delta_{n,m} \tag{16}$$

which corresponds to the spectral problem of the Hermitian Hubbard model in the two-particle sector under OBC. In the large L limit, the energy spectrum remains entirely real and is thus given by Equations (9) and (10) and depicted in Figure 2. In other words, like in the Hatano-Nelson model under OBC the energy spectrum is not modified by the application of the imaginary gauge field h, however according to Equation (15) the eigenstates are squeezed toward the corner $n = m = 0$, corresponding to the non-Hermitian skin effect for the two interacting particles.

3.2. Energy Spectrum on the Infinite Lattice

In the infinite lattice, we can solve the spectral problem defined by Equations (8) and (12) using the same procedure as in the Hermitian Hubbard model, decomposing the wave function in terms of the center of mass and relative spatial coordinates (see e.g., [6]). After letting

$$u_{n,m} = \Phi_{n-m}\exp[iq(n + m)] \tag{17}$$

for $m \le n$, and $u_{n,m} = u_{m,n}$ for $m \ge n$, from Equation (8) one obtains the following difference equation for the amplitudes Φ_l, with $l = n - m$ the relative spatial coordinate between the two fermions

$$E\Phi_l = -2J\sigma(\Phi_{l+1} + \Phi_{l-1}) + U\delta_{l,0}\Phi_0 \tag{18}$$

and $\Phi_l = \Phi_{-l}$. In the above equation we have set

$$\sigma \equiv \cos(q - ih) \tag{19}$$

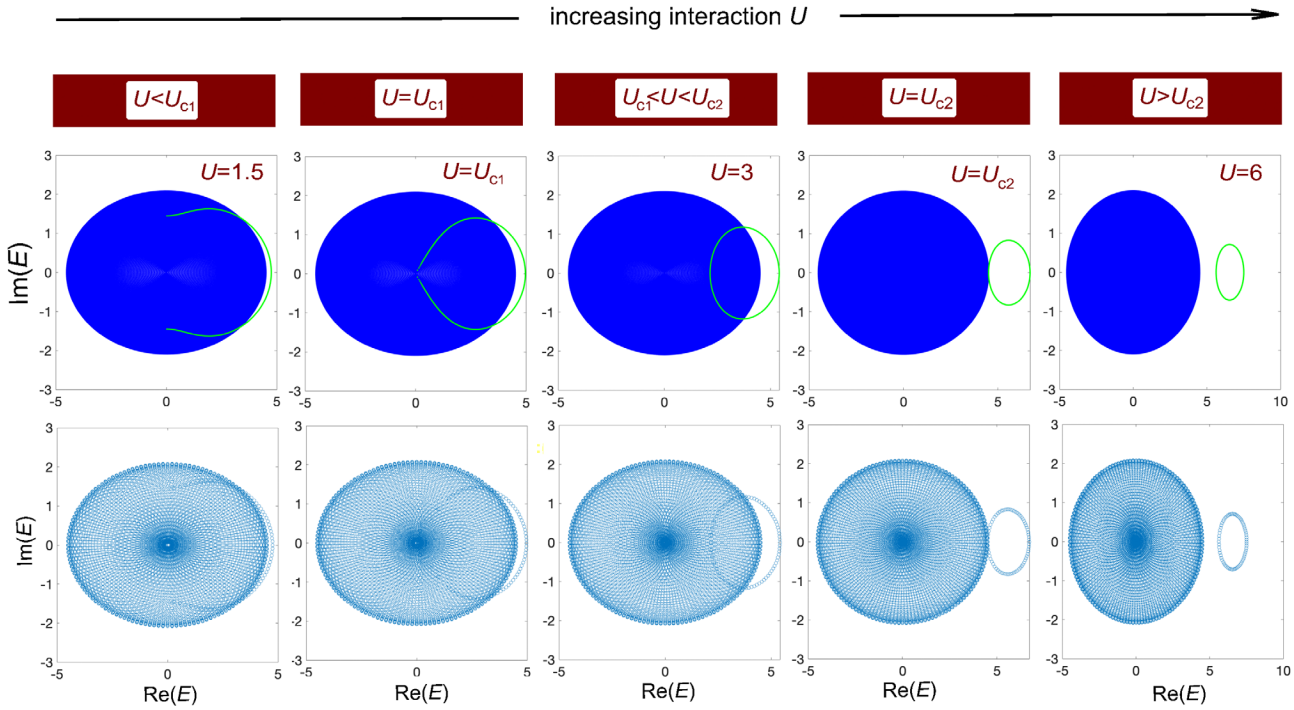

Figure 3. Energy spectrum $\sigma(H_{1LL})$ of the two-particle non-Hermitian Hubbard model on an infinite lattice for increasing interaction energy U. Parameter values are $J = 1$ and $h = 0.5$. The critical values of the interaction energy U_{c1} and U_{c2} are given by Equations (22) and (23), and for the specific parameter values read $U_{c1} \simeq 2.0844$ and $U_{c2} \simeq 4.9688$. The upper row shows the energy spectra (E_1- and E_2-energy branches) as obtained by the exact analysis. The shaded area, independent of U, describes the energy spectrum of the scattered two-particle states [Equation (20), E_1 branch], whereas the solid light curve describes the doublon (Mott-Hubbard) energy band [Equation (21), E_2 branch]. For $U < U_{c1}$ ($U > U_{c1}$) the Mott-Hubbard band describes an open (closed) loop in complex energy plane. For $U > U_{c2}$ a line gap separates the two bands. The lower row shows the energy spectra as computed by numerical diagonalization of the matrix Hamiltonian in a finite lattice comprising $L = 70$ sites and assuming PBC.

and the parameter $q = (k_1 + k_2)/2$ in Equation (17) plays the role of the quasi-momentum of the center of mass of the two fermions. Clearly, the asymptotic condition (12) requires q to be a real number. The eigenstates and corresponding energy spectra of Equation (18), which are bounded as $l \to \pm\infty$, are calculated in Appendix A and consists of two branches (E_1- and E_2-energy branches)i) a set of scattered states with asymptotic behavior $\Phi_l \approx \cos(Ql)$ as $l \to \infty$, where $Q = (k_1 - k_2)/2$ is an arbitrary real parameter, which physically describes the quasi-momentum of the relative particle motion; and (ii) a set of bound states, namely $\Phi_l = \exp(-\mu|l|)$ ($l \neq 0$) with $\mu > 0$, corresponding to the bounded two-particle state (doublon) branch. The dispersion curve of the scattered two-particle states (E_1-energy branch) is given by

$$E_1 = -4J\cos(q - ih)\cos Q = -2J\cos(k_1 - ih) - 2J\cos(k_2 - ih) \tag{20}$$

whereas the dispersion curve of the bound two-particle states (E_2-energy branch) reads

$$E_2 = \sqrt{U^2 + 16J^2\cos^2(q - ih)} \tag{21}$$

Note that the two above energy branches can be obtained from the corresponding dispersion curves in the Hermitian limit [Equations (9) and (10)] after the substitution $k_{1,2} \to k_{1,2} - ih$ and $q \to q - ih$. Typical examples of the energy spectra for increasing values of the interaction energy U, as given by the analytical expression Equations (20) and (21), are shown in the upper row of **Figure 3**. For comparison, the energy spectra numerically computed in a finite lattice of size $L = 70$ by matrix diagonalization and applying PBC are depicted in the lower row of Figure 3, indicating that the analytical results well approximate the PBC energy spectra in the large L limit. Note that the energy spectra associated to the two-particle scattered states cover an entire area of the complex energy plane. Clearly, this result also occurs for non-interacting particles and is due to the fact that we are dealing with two particles and the energy dispersion curve E_1 depends on two real parameters k_1 and k_2. The fact that the two-particle energy spectrum is described by an area in complex plane is the clear signature of the non-Hermitian skin effect.[54] On the other hand, the energy spectrum associated to the two-particle bound states (doublon) is described by a curve in complex energy plane, since in this case the dispersion curve of the E_2-energy branch depends only on one real parameter $q = (k_1 + k_2)/2$. It can be readily shown that such a curve describes an open arc when $U < U_{c1}$, whereas it describes a closed loop when $U > U_{c1}$, where the critical interaction energy U_{c1} is given by

$$U_{c1} = 4J\sinh h \tag{22}$$

Therefore, the doublon (Mott-Hubbard) E_2-energy branch shows a first spectral phase transition as U is increased above U_{c1}. The fact that for $U < U_{c1}$ the energy spectrum of the Mott-Hubbard

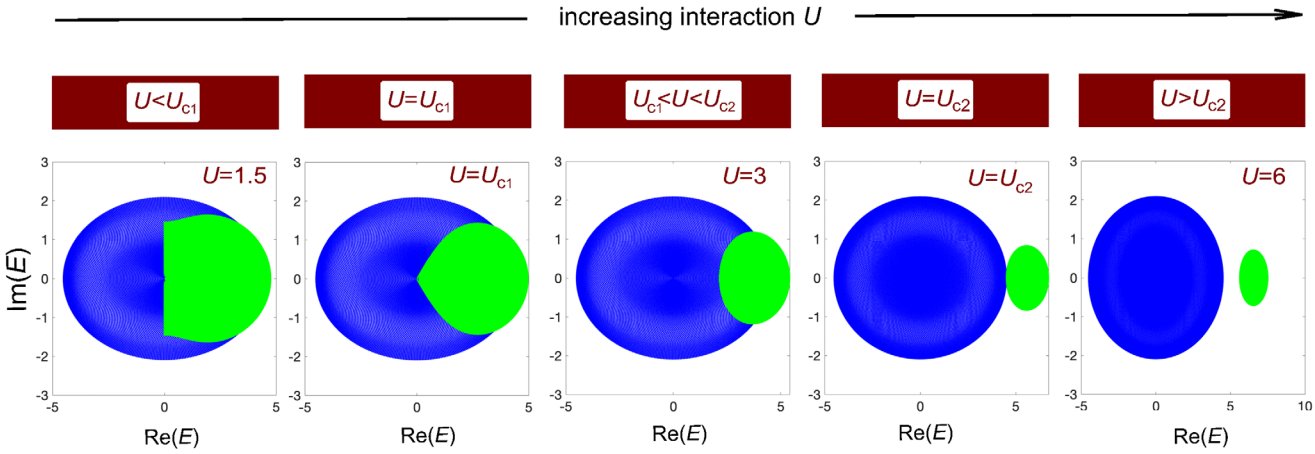

Figure 4. Energy spectrum $\sigma(H_{SIBC})$ of the two-particle non-Hermitian Hubbard model on an semi-infinite lattice for increasing interaction energy U. Parameter values are as in Figure 3 ($J = 1$, $h = 0.5$). The dark shaded area, independent of U, describes the E_1 energy branch, whereas the light shaded area describes the spectrum of the doublon eigenstates (E_2 branch). The critical values U_{c1} and U_{c2} are given by Equations (22) and (23).

band describes an open (rather than a closed) loop is a rather unexpected and remarkable result, since in single-particle models displaying the non-Hermitian skin effect the energy spectra are described by open loops with a nontrivial point-gap topology.

At a larger interaction strength U_{c2}, given by

$$U_{c2} = 4J\sqrt{\cosh^2 h + \sinh^2 h} \tag{23}$$

the Mott-Hubbard spectral loop E_2 fully detaches from the scattered two-particle energy spectrum E_1, which are separated one other by a line gap. This behavior is clearly illustrated in the upper row of Figure 3. While the detachment of the Mott-Hubbard band as the interaction energy U is increased above the critical value U_{c2} is similar to the behavior found in the ordinary (Hermitian) Hubbard model (see Figure 2), the spectral phase transition of the Mott-Hubbard band occurring at the lower interaction energy U_{c1}, from an open to a closed loop in the complex energy plane, is a purely non-Hermitian phenomenon without any counterpart in the Hermitian Hubbard model.

3.3. Energy Spectrum on the Semi-Infinite Lattice

The energy spectrum on the semi-infinite lattice $\sigma(H_{SIBC})$ requires to solve the spectral problem defined by Equations (8), (13), and (14). As compared to the infinite lattice case considered in the previous subsection, the analysis is more involved and the technical details are given in the Appendix B. The starting point is provided by a Bethe-like Ansatz[3,83] of the wave function $u_{n,m}$, given by the superposition of eight plane waves obtained by the set of permutations of the complex wave numbers $\pm k_1$ and $\pm k_2$ for the two particles, suitably modified to account for a non-vanishing imaginary gauge field h. As shown in the Appendix B and illustrated in **Figure 4**, the energy spectrum consists of two branches. The first branch (E_1-energy branch) is defined by the dispersion relation

$$E_1 = -2J\cos(k_1 - ih) - 2J\cos(k_2 - ih) \tag{24}$$

which is formally the same as the dispersion curve of two-particle scattered states found in the infinite lattice case [Equation (20)]. However, under SIBC the wave numbers k_1 and k_2 can be complex and should satisfy the minimal constraint

$$0 \leq \mathrm{Im}(k_{1,2}) \leq 2h \tag{25}$$

By restricting k_1 and k_2 to be real, i.e., for $\mathrm{Im}(k_{1,2}) = 0$, we retrieve the E_1-energy branch on the infinite lattice derived in Section 3.2 and corresponding to scattered two-particle states. Remarkably, under SIBC even though we allow the imaginary parts of k_1 and k_2 to be non vanishing and to vary in the range constrained by Equation (25), the E_1-branch of the energy spectrum does not change and describes the same area in complex energy plane as in the infinite lattice case (see the shaded dark areas in Figures 3 and 4, which are the same and independent of U). However, when the imaginary parts of k_1 and k_2 do not vanish, the wave functions are not anymore extended (scattered states), rather they become squeezed toward the edge $n = m = 1$ (two-particle non-Hermitian skin effect). Finally, we note that by restricting $\mathrm{Im}(k_{1,2}) = h$, the E_1 branch of the SIBC energy spectrum reduces to the E_1-branch of the OBC energy spectrum [Equation (9)].

The second branch of the SIBC energy spectrum, the E_2-branch, is defined by the dispersion relation

$$E_2 = \sqrt{U^2 + 16J^2\cos^2(q - ih)} \tag{26}$$

which is formally the same as the E_2 branch on the infinite lattice [Equation (21)]. However, under SIBC the wave number $q = (k_1 + k_2)/2$ is allowed to have a non-vanishing imaginary part, satisfying the minimal constraint

$$0 \leq \mathrm{Im}(q) \leq h \tag{27}$$

As a consequence, while the E_2-energy branch in the infinite lattice is described by an open arc or a closed loop (Figure 3), under SIBC the E_2-energy branch describes an area in complex energy plane, as shown in Figure 4. Since the Mott-Hubbard

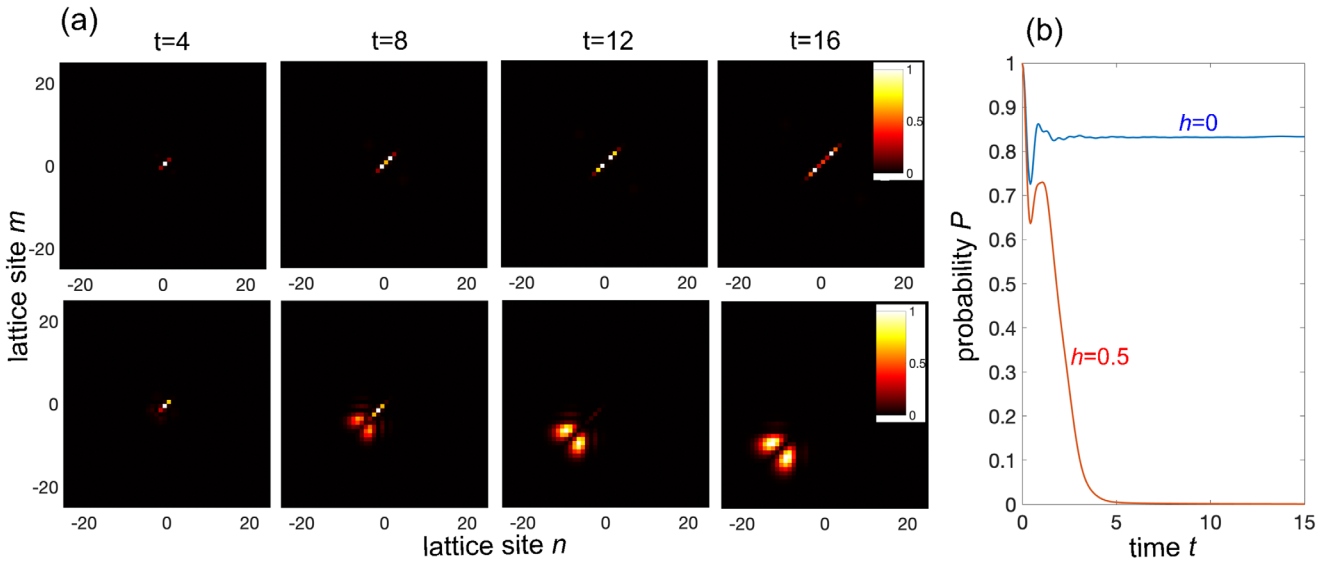

Figure 5. Dynamical behavior of the two-particle non-Hermitian Hubbard model. a) Temporal evolution of the two-particle occupation probabilities $|\psi_{n,m}(t)|^2$ on the lattice as obtained by numerical integration of Equations (4) for the initial condition $\psi_{n,m}(0) = \delta_{n,0}\delta_{m,0}$, corresponding to the two fermions occupying the same lattice site $n = 0$. Parameter values are $J = 1$, $U = 6$, and $h = 0$ (Hermitian limit, upper panels) and $h = 0.5$ (lower panels). The occupation probabilities are plotted using a pseudocolor map and, at each time instant, they are normalized to the peak value. The lattice size is large enough ($L = 51$) to avoid edge effects up to the largest observation time $t = 16$. b) Corresponding temporal evolution of the same-site occupation probability $P(t)$.

E_2-energy branch emerges only when the interaction energy U is non-vanishing, we can conclude that while in the interaction-free regime $U = 0$ the two energy spectra $\sigma(H_{ILL})$ and $\sigma(H_{SIBB})$ are the same, particle interaction lifts such degeneracy and the two spectra differ from one another under the two different boundary conditions.

4. Two-Particle Dynamics: Non-Hermitian Induced Doublon Dissociation and Burst Edge Revival

One of the major results of the Hubbard model in the Hermitian limit is the formation of stable pairs of bound particles occupying the same lattice site, dubbed doublons.[5–12] For sufficiently strong interactions, isolated doublons represent stable quasiparticles, which undergo correlated tunneling on the lattice.[13,14] Doublon dynamics has been experimentally observed using different platforms, such as ultracold atoms[5,13,14,68] and classical systems.[70,71] A natural question is whether two strongly-interacting particles remain bounded and undergo correlated tunneling on the lattice when we apply the non-Hermitian gauge field.

The *bulk* dynamical properties of the two-particle system, i.e., far from lattice edges, can be captured by expanding the state vector of the system on the basis of the eigenstates of the two-particle Hamiltonian on the infinite lattice,[34,76,84] with amplitudes given in terms of the scalar products of the initial state with the left eigenstates of the Hamiltonian. In our case, left and right eigenstates are just obtained from one another by a sign flip of h, i.e., by the transformation $h \to -h$. The resulting asymptotic dynamics is dominated by the eigenstates with the longer lifetime (for decaying states) or the larger growth rate (for unstable growing states).[34,76,84,85] The energy spectra shown in Figure 3 clearly show that the dominant eigenstates, with the largest growth rate, belong to the E_1-energy branch and thus they describe dissociated particle states, i.e., fermions that do not occupy the same lattice site. This means that, even for a strong interaction energy, two fermions with opposite spins initially placed at the same lattice site and forming a doublon state do not remain bounded any longer and they dissociate in the long time evolution. In other words, non-Hermiticity makes doublons unstable quasi-particle states. This result is clearly illustrated in **Figure 5**. The figure shows the numerically-computed temporal evolution of the two-particle probability occupation probabilities $|\psi_{n,m}(t)|^2$ [panel (a)] and of the probability $P(t)$ that the two fermions at time t occupy the same lattice site [panel(b)], i.e.,

$$P(t) = \sum_n |\psi_{n,n}(t)|^2 \tag{28}$$

At initial time, the two fermions are placed at the same site $n = 0$ of the lattice. While in the Hermitian limit the probability $P(t)$ reaches a stationary and large value, indicating the stability of the doublon state, in the non-Hermitian regime the probability $P(t)$ rapidly decays toward zero, indicating particle dissociation. It should be mentioned that particle dissociation shown in Figure 5 and induced by the imaginary gauge field is a very distinct phenomenon than non-Hermitian delocalization found in the Hatano-Nelson model with lattice disorder.[73–75] Delocalization concerns with the extended nature of either single-particle or two-particle eigenstates; in presence of disorder, single- and two-particle states that are Anderson localized undergoes a delocalization transition when an imaginary gauge field is applied. On the other hand, dissociation concerns the lifetime (rather than localized or extended nature) of the two-particle wave

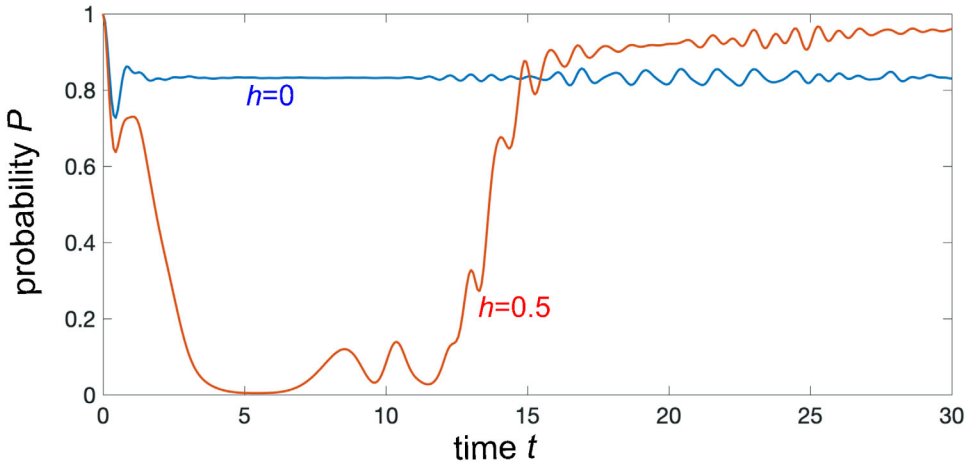

Figure 6. Edge burst revival of the same-site occupation probability $P(t)$ due to boundary effects. The figure shows the behavior of the probability $P(t)$ for the same parameter values as in Figure 5b, but on a finite lattice comprising $L = 31$ sites. When the two particles reach the lattice boundary, a sudden revival of $P(t)$ is observed in the non-Hermitian regime.

functions. In our model, we do not have any disorder in the system and so all states are delocalized, even when the imaginary gauge field h vanishes: so dynamical delocalization is observed for both single- and two-particle states. Dissociation of doublon states observed in Figure 5 is not related to delocalization, rather it originates physically from the larger growth rates of asymptotically-free two-particle states than those of two-particle bound states. This is because, when the two particles are sticked together, correlated tunneling occurs and spreading of bound states in the lattice is slower than that of single-particle states.[86] Correspondingly, when the left/right hopping rates are non-reciprocal, two-particle bound state wave packets (doublons) experience a lower amplification than asymptotically-free two-particle wave packets when they drift and spread along the bulk of the lattice, resulting in the effective dissociation of the particles under continuous measurements of the system. It should be mentioned that with additional non-Hermitian terms in the Hubbard model, for example by including an additional two-particle gain term by replacing U with $U + iG$ ($G > 0$) in the last term of Equation (1), the growth rates of doublon states could become larger than those of asymptotically-free two-particle states, so that in such a regime doublons do not dissociate, the two particles remain sticked together, yet the bound state wave packet spreads and delocalizes in the lattice.

The doublon dissociation shown in Figure 5 is clearly a bulk dynamical phenomenon. Remarkably, when the particles reach the boundaries of the lattice a burst revival of $P(t)$, corresponding to a sudden resurgence of the doublon state, is observed, as shown in **Figure 6**. Such an edge burst revivial is a striking boundary-induced dynamical phenomenon peculiar to non-Hermitian systems displaying the non-Hermitian skin effect, and extend to correlated particle systems, edge burst dynamical phenomena predicted and observed in single-particle non-Hermitian models.[51,52] From a physical viewpoint, the edge resurgence of the doublon state provides a clear and experimentally-accessible dynamical manifestation of the boundary-dependent energy spectrum of the two-particle non-Hermitian Hubbard model.

5. Conclusion

Non-Hermitian systems exhibit a variety of intriguing phenomena that lack Hermitian counterparts, such as the strong dependence of the energy spectrum on the boundary conditions, the anomalous accumulation of bulk modes at the edges (non-Hermitian skin effect), non-trivial point-gap topologies, and a wide variety of exotic bulk and edge dynamical phenomena. The physics of strongly-correlated systems described by effective non-Hermitian Hamiltonians has attracted a great interest recently, owing to the unique and largely unexplored properties arising from the interplay between particle correlations and non-Hermitian skin effect, such as non-Hermitian many-body localization and a nontrivial many-body topology. The interacting Hatano-Nelson model provides one of the simplest non-Hermitian extensions of the Hubbard model, which is a cornerstone theoretical model in condensed matter physics of strongly-correlated systems. In this work, we presented exact analytical results of the spectral structure of the interacting Hatano-Nelson model in the two-particle sector of Hilbert space under different boundary conditions and unravelled emerging spectral and dynamical effects arising from the interplay between particle correlation and non-Hermitian terms in the Hamiltonian. These include i) a novel spectral phase transition of the Mott-Hubbard band on the infinite lattice, from an open to a closed loop in complex energy plane; ii) a correlation-induced lifting of degeneracy between spectra on the infinite and semi-infinite lattices; iii) dynamical dissociation of doublons, i.e., instability of two-particle bound states, in the bulk of the lattice; and iv) a burst revival of the doublon state when the two particles reach the lattice edge. The latter phenomenon is a striking boundary-induced dynamical phenomenon peculiar to non-Hermitian systems displaying the non-Hermitian skin effect, and should provide an experimentally-accessible dynamical signature of the boundary-dependent energy spectrum of the two-particle non-Hermitian Hubbard model. Our results shed new physical insights into the simplest non-Hermitian extension of the Hubbard model in the few-particle regime, highlight the strong

impact of non-Hermiticity on the spectral and dynamical features of two strongly-correlated particles, and should stimulate further theroertical and experimental studies on an emergent area of research.[87]

Appendix A: Energy Spectrum on the Infinite Lattice

The calculation of the eigenstates and corresponding energy spectrum on the infinite lattice entails to determine the eigenfunctions Φ_l of the difference equation [Equation (18) in the main text]

$$E\Phi_l = -2\sigma J(\Phi_{l+1} + \Phi_{l-1}) + U\Phi_l\delta_{l,0} \tag{A1}$$

with $\Phi_{-l} = \Phi_l$ and with the asymptotic condition that $|\Phi_l|$ is bounded as $l \to \infty$. In the above equation, we have set

$$\sigma = \cos(q - ih) \tag{A2}$$

which is parametrized by the real parameter $q = (k_1 + k_2)/2$, corresponding to the quasi momentum of the particle center of mass. The spectral problem defined by Equation (A1) with the appropriate boundary conditions corresponds to the well-known single-particle scattering problem on a lattice from a single impurity, but with a *complex* hopping amplitude $2J\sigma$. The solutions to the single-impurity problem, bounded as $l \to \infty$, comprise two types of states.

(i) *Scattered states*, i.e., states that are bounded but do not vanish, i.e., oscillate, as $l \to \infty$. They are given by

$$\Phi_l = \begin{cases} \sum_{\pm}\left(\frac{1}{2} \pm \frac{U}{8i\sigma J \sin Q}\right)\exp(\pm iQ|l|) & l \neq 0 \\ 1 & l = 0 \end{cases} \tag{A3}$$

and the corresponding eigenenergies are

$$E_1 = -4\sigma J \cos Q \tag{A4}$$

where $Q = (k_1 - k_2)/2$ is an arbitrary real parameter, corresponding to the quasi momentum of the relative particle motion. Substitution of Equation (A2) into Equation (A4) yields

$$E_1 = -4J\cos Q\cos(q - ih) = -2J\cos(k_1 - ih) - 2J\cos(k_2 - ih) \tag{A5}$$

which is the energy branch of two-particle scattered states given by Equation (20) in the main text.

(i) *Bound states*, i.e., states such that $\Phi_l \to 0$ as $l \to \infty$. It can be readily shown that the eigenstates corresponding to bound modes are given by

$$\Phi_l = \begin{cases} \frac{U-E}{4\sigma J\exp(-\mu)}\exp(-\mu|l|) & l \neq 0 \\ 1 & l = 0 \end{cases} \tag{A6}$$

with corresponding eigenenergies

$$E_2 = -2\sigma J\cosh\mu. \tag{A7}$$

In the above equations, the complex parameter μ is given by

$$\mu = \log\left(-\frac{U}{4\sigma J} \pm \sqrt{1 + \left(\frac{U}{4\sigma J}\right)^2}\right) \tag{A8}$$

where the sign on the right hand side of Equation (A8) should be chosen such that $\mathrm{Re}(\mu) > 0$. Substitution of Equation (A8) into Equation (A7) yields

$$E_2 = \sqrt{U^2 + 16J^2\sigma^2} = \sqrt{U^2 + 16J^2\cos^2(q - ih)} \tag{A9}$$

which is the energy of the two-particle bound states given by Equation (21) in the main text.

Appendix B: Energy Spectrum on the Semi-Infinite Lattice

The spectral problem of the two-particle non-Hermitian Hubbard model on a semi-infinite lattice is defined by Equations (8) with the boundary conditions (13) and (14). In the spirit of the Bethe Ansatz,[3,81–83] generalized to account for the imaginary gauge field h, we may look for a solution to Equations (8) of the form

$$\begin{aligned} u_{n,m} = {} & A_1\exp(ik_1n + ik_2m) + A_2\exp(-ik_1n + ik_2m - 2hn) \\ & + A_3\exp(ik_1n - ik_2m - 2hm) \\ & + A_4\exp(-ik_1n - ik_2m - 2hn - 2hm) \\ & + A_5\exp(ik_2n + ik_1m) + A_6\exp(-ik_2n + ik_1m - 2hn) \\ & + A_7\exp(ik_2n - ik_1m - 2hm) \\ & + A_8\exp(-ik_2n - ik_1m - 2hn - 2hm) \end{aligned} \tag{B1}$$

for $n = 1, 2, 3, \ldots$ and $1 \leq m \leq n$, with $u_{n,m} = u_{m,n}$ for $m \geq n$ and with the corresponding eigenenergy E given by

$$E = -2J\cos(k_1 - ih) - 2J\cos(k_2 - ih) \tag{B2}$$

In Equation (B1), the amplitudes A_l should be determined by imposing the boundary condition $u_{n,0} = 0$ for $n = 1, 2, 3, \ldots$ and the validity of Equations (8) for $n = m$, whereas the only constraint for the complex wave numbers k_1 and k_2 is the boundedness condition (14) of the wave function as $n, m \to +\infty$. To solve the spectral problem, we should distinguish two cases, that correspond in the Hermitian limit $h = 0$ to the energy spectra of the two-particle scattered states (E_1 energy branch) and of the two-particle bound states (E_2 energy branch).

(i) E_1-energy branch. In this case, all amplitudes A_l ($l = 1, 2, \ldots, 8$) in Equation (B1) are non-vanishing. After imposing the boundary condition $u_{n,0} = 0$ for $n = 1, 2, 3, \ldots$ and the validity of Equations (8) for $n = m$, one obtains the following set of linear homogeneous equations for the vector $\mathbf{A} = (A_1, A_2, \ldots, A_8)^T$ of the wave amplitudes

$$\mathcal{M}\mathbf{A} = 0 \tag{B3}$$

where the non-vanishing elements of the 8×8 matrix $\mathcal{M}$ are given by

$$\mathcal{M}_{11} = \mathcal{M}_{13} = \mathcal{M}_{22} = \mathcal{M}_{24} = \mathcal{M}_{35} = \mathcal{M}_{37} = \mathcal{M}_{46} = \mathcal{M}_{48} = 1$$

$$\mathcal{M}_{51} = E - U + 2J\exp(h + ik_1) + 2J\exp(-h - ik_2)$$

$$\mathcal{M}_{55} = E - U + 2J\exp(h + ik_2) + 2J\exp(-h - ik_1)$$

$$\mathcal{M}_{62} = E - U + 2J\exp(-h - ik_1) + 2J\exp(-h - ik_2)$$

$$\mathcal{M}_{67} = E - U + 2J\exp(h + ik_2) + 2J\exp(h + ik_1)$$

$$\mathcal{M}_{73} = E - U + 2J\exp(h + ik_1) + 2J\exp(h + ik_2) = \mathcal{M}_{67}$$

$$\mathcal{M}_{76} = E - U + 2J\exp(-h - ik_2) + 2J\exp(-h - ik_1) = \mathcal{M}_{62}$$

$$\mathcal{M}_{84} = E - U + 2J\exp(-h - ik_1) + 2J\exp(h + ik_2) = \mathcal{M}_{55}$$

$$\mathcal{M}_{88} = E - U + 2J\exp(-h - ik_2) + 2J\exp(h + ik_1) = \mathcal{M}_{51} \quad \text{(B4)}$$

It can be readily shown that, for arbitrary complex wave numbers $k_{1,2}$, one has $\det \mathcal{M} = 0$. This means that there exist non-trivial solutions to the spectral problem for arbitrary values of $k_{1,2}$, the only constraint being given by the boundedness condition (14). From Equation (B1), it readily follows that the wave function $u_{n,m}$ is bounded as $n, m \to +\infty$ provided that

$$0 \leq \mathrm{Im}(k_{1,2}) \leq 2h \quad \text{(B5)}$$

Therefore, the first branch E_1 of the energy spectrum is given by Equation (B2), where k_1 and k_2 are arbitrary complex wave numbers satisfying the only constraint given by Equation (B5). Note that, if we restrict k_1 and k_2 to be real, i.e., $\mathrm{Im}(k_{1,2}) = 0$, the E_1-energy branch under SIBC reproduces the E_1-branch on the infinite lattice derived in Section 3.2 and corresponding to scattered two-particle states. Remarkably, even though we allow the imaginary parts of k_1 and k_2 to be non vanishing and to vary in the range constrained by Equation (B5), the E_1-energy spectrum is not changed and describes the same area in the complex energy plane as in the infinite lattice case (see the shaded dark areas of Figures 3 and 4). However, when the imaginary parts of k_1 and k_2 do not vanish, the wave functions are squeezed toward the edge $n = m = 1$, corresponding to the two-particle non-Hermitian skin effect.

(ii) E_2-energy branch. A different type of solutions is found by assuming $A_2 = A_4 = A_5 = A_7 = 0$, so that the plane-wave expansion (B1) contains only four components $\mathrm{A}' = (A_1, A_3, A_6, A_8)^T$. The boundedness condition for the wave function $u_{n,m}$ as $n, m \to +\infty$ is met provided that

$$0 \leq \mathrm{Im}(k_1) \leq 2h \ , \quad -\mathrm{Im}(k_1) \leq \mathrm{Im}(k_2) \leq 2h. \quad \text{(B6)}$$

Unlike the previous case, in order for the homogeneous system Equation (B3) to have non-trivial solutions it can be readily shown that the following solvability condition

$$U = 4iJ\sin\left(\frac{k_1 - k_2}{2}\right)\cos\left(\frac{k_1 + k_2}{2} - ih\right) \quad \text{(B7)}$$

should be satisfied. The solvability condition (B7) basically indicates that the two variables $Q \equiv (k_1 - k_2)/2$ and $q \equiv (k_1 + k_2)/2$ cannot be chosen independently one another: once one of the two variables has been arbitrarily chosen, with the only constraint imposed by the boundedness of the wave function $u_{n,m}$ at infinity [Equation (B6)], the other one is determined via Equation (B7). Let us assume

$$q \equiv \frac{k_1 + k_2}{2} \quad \text{(B8)}$$

as the independent variable. The boundedness condition (B6) yields the constraint $0 \leq \mathrm{Im}(q) \leq 2h$. The corresponding eigenenergy of the E_2-branch is given by Equation (B2), which using Equation (B7) can be written in the following form

$$\begin{aligned} E_2 &= -2J\cos(k_1 - ih) - 2J\cos(k_2 - ih) \\ &= -4J\cos(q - ih)\cos(Q) = 4J\cos(q - ih)\sqrt{1 - \sin^2 Q} \\ &= \sqrt{U^2 + 16J^2\cos^2(q - ih)} \end{aligned} \quad \text{(B9)}$$

Note that Equation (B9) is formally the same as Equation (A9) describing the energy dispersion curve of the Mott-Hubbard band on the infinite crystal, however while in the latter case the wave number q must be real under SIBC q is a complex number with the minimal constraint $0 \leq \mathrm{Im}(q) \leq 2h$.

Acknowledgements

The author acknowledges the Spanish State Research Agency, through the Severo Ochoa and Maria de Maeztu Program for Centers and Units of Excellence in R&D (Grant no. MDM-2017-0711).

Conflict of Interest

The authors declare no conflict of interest.

Data Availability Statement

Data sharing is not applicable to this article as no new data were created or analyzed in this study.

Keywords

hubbard model, non-hermitian physics, non-hermitian skin effect, strongly-correlated systems

Received: June 21, 2023
Revised: July 20, 2023
Published online:

[1] J. Hubbard, *Proc. R. Soc. Lond. Ser. A Math. Phys. Sci.* **1963**, *276*, 238.
[2] H. Tasaki, *J. Phys.: Condens. Matter* **1998**, *10*, 4353.
[3] F. H. L. Essler, H. Frahm, F. Göhmann, A. Klümper, V. E. Korepin, *The One-Dimensional Hubbard Model*, Cambridge University Press, Cambridge **2005**.
[4] D. P. Arovas, E. Berg, S. A. Kivelson, S. Raghu, *Annu. Rev. Condens. Matter Phys.* **2022**, *13*, 239.
[5] K. Winkler, G. Thalhammer, F. Lang, R. Grimm, J. Hecker Denschlag, A. J. Daley, A. Kantian, H. P. Büchler, P. Zoller, *Nature* **2006**, *441*, 853.
[6] M. Valiente, D. Petrosyan, *J. Phys. B* **2008**, *41*, 161002.
[7] N. Strohmaier, D. Greif, R. Jördens, L. Tarruell, H. Moritz, T. Esslinger, R. Sensarma, D. Pekker, E. Altman, E. Demler, *Phys. Rev. Lett.* **2010**, *104*, 080401.
[8] F. Hofmann, M. Potthoff, *Phys. Rev. B* **2021**, *85*, 205127.
[9] A. L. Chudnovskiy, D. M. Gangardt, A. Kamenev, *Phys. Rev. Lett.* **2012**, *108*, 085302.
[10] S. Longhi, G. Della Valle, *Phys. Rev. B* **2013**, *87*, 013634.
[11] L. Xia, L. A. Zundel, J. Carrasquilla, A. Reinhard, J. M. Wilson, M. Rigol, D. S. Weiss, *Nat. Phys.* **2015**, *11*, 316.
[12] K. Balzer, M. Rodriguez Rasmussen, N. Schlünzen, J.-P. Joost, M. Bonitz, *Phys. Rev. Lett.* **2018**, *121*, 267602.
[13] S. Trotzky, P. Cheinet, S. Fölling, M. Feld, U. Schnorrberger, A. M. Rey, A. Polkovnikov, E. A. Demler, M. D. Lukin, I. Bloch, *Science* **2008**, *319*, 295.
[14] Y.-A. Chen, S. Nascimbene, M. Aidelsburger, M. Atala, S. Trotzky, I. Bloch, *Phys. Rev. Lett.* **2011**, *107*, 210405.
[15] Y. Ashida, Z. Gong, M. Ueda, *Adv. Phys.* **2021**, *69*, 249.
[16] Z. Gong, Y. Ashida, K. Kawabata, K. Takasan, S. Higashikawa, M. Ueda, *Phys. Rev. X* **2018**, *8*, 031079.
[17] K. Kawabata, K. Shiozaki, M. Ueda, M. Sato, *Phys. Rev. X* **2019**, *9*, 041015.
[18] E. J. Bergholtz, J. C. Budich, F. K. Kunst, *Rev. Mod. Phys.* **2021**, *93*, 15005.
[19] X. Zhang, T. Zhang, M.-H. Lu, Y.-F. Chen, *Adv. Phys. X* **2022**, *7*, 2109431.
[20] K. Ding, C. Fang, G. Ma, *Nat. Rev. Phys.* **2022**, *4*, 745.

[21] A. Banerjee, R. Sarkar, S. Dey, A. Narayan, *J. Phys.: Condens. Matter.* **2023**, *35*, 333001.
[22] R. Lin, T. Tai, L. Li, C.-H. Lee, *Front. Phys.* **2023**, *18*, 53605.
[23] T. E. Lee, *Phys. Rev. Lett.* **2016**, *116*, 133903.
[24] D. Leykam, K. Y. Bliokh, C. Huang, Y. D. Chong, F. Nori, *Phys. Rev. Lett.* **2017**, *118*, 040401.
[25] H. Shen, B. Zhen, L. Fu, *Phys. Rev. Lett.* **2018**, *120*, 146402.
[26] F. K. Kunst, E. Edvardsson, J. C. Budich, E. J. Bergholtz, *Phys. Rev. Lett.* **2018**, *121*, 026808.
[27] S. Yao, Z. Wang, *Phys. Rev. Lett.* **2018**, *121*, 086803.
[28] S. Yao, F. Song, Z. Wang, *Phys. Rev. Lett.* **2018**, *121*, 136802.
[29] C. H. Lee, R. Thomale, *Phys. Rev. B* **2019**, *99*, 201103.
[30] C. H. Lee, L. Li, J. Gong, *Phys. Rev. Lett.* **2019**, *123*, 016805.
[31] K. Yokomizo, S. Murakami, *Phys. Rev. Lett.* **2019**, *123*, 066404.
[32] T. Liu, Y.-R. Zhang, Q. Ai, Z. Gong, K. Kawabata, M. Ueda, F. Nori, *Phys. Rev. Lett.* **2019**, *122*, 076801.
[33] L. Herviou, J. H. Bardarson, N. Regnault, *Phys. Rev. A* **2019**, *99*, 052118.
[34] S. Longhi, *Phys. Rev. Res.* **2019**, *1*, 023013.
[35] K.-I. Imura, Y. Takane, *Phys. Rev. B* **2019**, *100*, 165430.
[36] L. Jin, Z. Song, *Phys. Rev. B* **2019**, *99*, 081103.
[37] S. Longhi, *Phys. Rev. Lett.* **2020**, *124*, 066602.
[38] Z. Yang, K. Zhang, C. Fang, J. Hu, *Phys. Rev. Lett.* **2020**, *125*, 226402.
[39] N. Okuma, K. Kawabata, K. Shiozaki, M. Sato, *Phys. Rev. Lett.* **2020**, *124*, 086801.
[40] N. Matsumoto, K. Kawabata, Y. Ashida, S. Furukawa, M. Ueda, *Phys. Rev. Lett.* **2020**, *125*, 260601.
[41] K. Zhang, Z. Yang, C. Fang, *Phys. Rev. Lett.* **2020**, *125*, 126402.
[42] L. Xiao, T. Deng, K. Wang, G. Zhu, Z. Wang, W. Yi, P. Xue, *Nat. Phys.* **2020**, *16*, 761.
[43] A. Ghatak, M. Brandenbourger, J. van Wezel, C. Coulais, *Proc Nat. Acad. Sci.* **2020**, *117*, 29561.
[44] T. Helbig, T. Hofmann, S. Imhof, M. Abdelghany, T. Kiessling, L. W. Molenkamp, C. H. Lee, A. Szameit, M. Greiter, R. Thomale, *Nat. Phys.* **2020**, *16*, 747.
[45] S. Weidemann, M. Kremer, T. Helbig, T. Hofmann, A. Stegmaier, M. Greiter, R. Thomale, A. Szameit, *Science* **2020**, *368*, 311.
[46] Y. Song, W. Liu, L. Zheng, Y. Zhang, B. Wang, P. Lu, *Phys. Rev. Appl.* **2020**, *14*, 064076.
[47] H. Hu, E. Zhao, *Phys. Rev. Lett.* **2021**, *126*, 010401.
[48] K. Kawabata, K. Shiozaki, S. Ryu, *Phys. Rev. Lett.* **2021**, *126*, 216405.
[49] X. Zhang, Y. Tian, J.-H. Jiang, M.-H. Lu, Y.-F. Chen, *Nat. Commun.* **2021**, *12*, 5377.
[50] S. Longhi, *Phys. Rev. Lett.* **2022**, *128*, 157601.
[51] W.-T. Xue, Y.-M. Hu, F. Song, Z. Wang, *Phys. Rev. Lett.* **2022**, *128*, 120401.
[52] L. Xiao, W.-T. Xue, F. Song, Y.-M. Hu, W. Yi, Z. Wang, P. Xue, *arXiv:2303.12831* **2023**.
[53] Q. Liang, D. Xie, Z. Dong, H. Li, H. Li, B. Gadway, W. Yi, B. Yan, *Phys. Rev. Lett.* **2022**, *129*, 070401.
[54] K. Zhang, Z. Yang, C. Fang, *Nat. Commun.* **2022**, *13*, 2496.
[55] R. Sarkar, A. Bandyopadhyay, A. Narayan, *Phys. Rev. B* **2023**, *107*, 035403.
[56] T. Fukui, N. Kawakami, *Phys. Rev. B* **1998**, *58*, 16051.
[57] R. Hamazaki, K. Kawabata, M. Ueda, *Phys. Rev. Lett.* **2019**, *123*, 090603.
[58] T. Liu, J. J. He, T. Yoshida, Z.-L. Xiang, F. Nori, *Phys. Rev. B* **2020**, *102*, 235151.
[59] L.-J. Zhai, S. Yin, G.-Y. Huang, *Phys. Rev. B* **2020**, *102*, 064206.
[60] S.-B. Zhang, M. M. Denner, T. Bzdusek, M. A. Sentef, T. Neupert, *Phys. Rev. B* **2022**, *106*, L121102.
[61] K. Kawabata, K. Shiozaki, S. Ryu, *Phys. Rev. B* **2022**, *105*, 165137.
[62] K. Suthar, Y.-C. Wang, Y.-P. Huang, H. H. Jen, J.-S. You, *Phys. Rev. B* **2022**, *106*, 064208.
[63] B. Dóra, C. P. Moca, *Phys. Rev. B* **2022**, *106*, 235125.
[64] T. Yoshida, Y. Hatsugai, *Phys. Rev. B* **2022**, *106*, 205147.
[65] R. Shen, C. H. Lee, *Commun. Phys.* **2022**, *5*, 238.
[66] T. Yoshida, Y. Hatsugai, *Phys. Rev. B* **2023**, *107*, 075118.
[67] a) L. Mao, Y. Hao, L. Pan, *Phys. Rev. A* **2023**, *107*, 043315; b) S. Sayyad, J. L. Lado, *Phys. Rev. Res.* **2023**, *5*, L022046.
[68] P. M. Preiss, R. Ma, M. E. Tai, A. Lukin, M. Rispoli, P. Zupancic, Y. Lahini, R. Islam, M. Greiner, *Science* **2015**, *347*, 1229.
[69] M. Schreiber, S. S. Hodgman, P. Bordia, H. P. Luschen, M. H. Fischer, R. Vosk, E. Altman, U. Schneider, I. Bloch, *Science* **2015**, *349*, 842.
[70] G. Corrielli, A. Crespi, G. Della Valle, S. Longhi, R. Osellame, *Nat. Commun.* **2013**, *4*, 1555.
[71] N. A. Olekhno, E. I. Kretov, A. A. Stepanenko, P. A. Ivanova, V. V. Yaroshenko, E. M. Puhtina, D. S. Filonov, B. Cappello, L. Matekovits, M. A. Gorlach, *Nat. Commun.* **2020**, *11*, 1436.
[72] W. Zhang, F. Di, H. Yuan, H. Wang, X. Zheng, L. He, H. Sun, X. Zhang, *Phys. Rev. B* **2022**, *105*, 195131.
[73] N. Hatano, D. R. Nelson, *Phys. Rev. Lett.* **1996**, *77*, 570.
[74] N. Hatano, D. R. Nelson, *Phys. Rev. B* **1997**, *56*, 8651.
[75] N. Hatano, D. R. Nelson, *Phys. Rev. B* **1988**, *58*, 8384.
[76] A. Panda, S. Banerjee, *Phys. Rev. B* **2020**, *101*, 184201.
[77] S. Lieu, *Phys. Rev. B* **2019**, *100*, 085110.
[78] N. Matsumoto, K. Kawabata, Y. Ashida, S. Furukawa, M. Ueda, *Phys. Rev. Lett.* **2020**, *125*, 260601.
[79] D.-W. Zhang, Y.-L. Chen, G.-Q. Zhang, L.-J. Lang, Z. Li, S.-L. Zhu, *Phys. Rev. B* **2020**, *101*, 235150.
[80] S. Longhi, *Proc. R. Soc. A* **2022**, *478*, 20210927.
[81] J. M. Zhang, D. Braak, M. Kollar, *Phys. Rev. Lett.* **2012**, *109*, 116405.
[82] J. M. Zhang, D. Braak, M. Kollar, *Phys. Rev. A* **2013**, *87*, 023613.
[83] S. Longhi, G. Della Valle, *J. Phys.: Condens. Matter.* **2013**, *25*, 235601.
[84] T. Hayata, Y. Hidaka, A. Yamamoto, *Prog. Theor. Exp. Phys.* **2023**, *2023*, 023I02.
[85] S. Weidemann, M. Kremer, S. Longhi, A. Szameit, *Nat. Photon.* **2021**, *15*, 576.
[86] S. Fölling, S. Trotzky, P. Cheinet, M. Feld, R. Saers, A. Widera, T. Müller, I. Bloch, *Science* **2007**, *448*, 1029.
[87] S. Longhi.,*Phys. Rev. B* **2023**, *108*, 075121.